

Article

Characterization of Atmospheric Iron Speciation and Acid Processing at Metropolitan Newark on the US East Coast

Guojie Xu ^{1,2,3,*} and Yuan Gao ³

¹ Collaborative Innovation Center on Forecast and Evaluation of Meteorological Disasters, Nanjing University of Information Science and Technology, Nanjing 210044, China

² Key Laboratory for Aerosol-Cloud-Precipitation of China Meteorological Administration, Nanjing University of Information Science & Technology, Nanjing 210044, China

³ Department of Earth and Environmental Sciences, Rutgers University, Newark, NJ 07102, USA; yuangaoh@newark.rutgers.edu

* Correspondence: hyssxuguojie@163.com

Academic Editor: Guey-Rong Sheu

Received: 7 March 2017; Accepted: 22 March 2017; Published: 24 March 2017

Abstract: To characterize atmospheric dissolved iron over Newark, a large metropolitan city on US east coast, size-segregated (0.056–18 μm in aerodynamic diameter) aerosols were collected in downtown Newark, New Jersey during August to October 2012. Aerosols samples were analyzed for Fe(II) and total dissolved iron (Fe(TD)) by UV/Visible spectroscopy, and water soluble compounds were analyzed by ion chromatograph (IC). Results from this study showed that Fe(II) concentrations were 2.1 ng m^{-3} (range: 1.2–4.2 ng m^{-3}), Fe(TD) concentrations were 2.4 ng m^{-3} (range: 1.3–4.9 ng m^{-3}). Dissolved iron (Fe(II) and Fe(TD)) in general appeared as bi-modal size distribution, was mainly accumulated in the fine mode. The highest concentration of dissolved iron displayed in the fine mode, which was associated with high concentrations of sulfate, oxalate and nitrate, suggesting the potential for Fe–acids interactions. Dissolved iron presented positive correlations with sulfate in the coarse mode, and with nitrate in the fine mode, further suggesting the importance of acid processing in aerosol iron solubility. However, as the oxalate concentration was so low, a good correlation between dissolved iron and oxalate in both the fine and coarse mode was not found.

Keywords: iron speciation; particle size; water soluble compounds; acid processing

1. Introduction

Fe exists in the atmosphere in one of two oxidation states, Fe(II) or Fe(III). Fe(II) is readily soluble in seawater and presumably bioavailable to marine phytoplankton [1]. The natural source of atmospheric Fe is aeolian dust derived from major deserts in Asia, North Africa, South America, and Australia that is transported and deposited to the ocean [2–5]. Atmospheric Fe may also come from anthropogenic sources, in particular from regions with heavy air pollution in the Northern Hemisphere. Major anthropogenic sources for Fe include agricultural practices [4], biomass burning [6,7] and combustion emissions [8–10]. Recent model results suggest that combustion-derived Fe can represent a large portion of soluble Fe fluxes, with the highest values (30%) close to the East Asian continent in the North Pacific [11].

Many atmospheric processes may affect Fe solubility, yielding Fe solubility over a wide range [12–15]. Dust particles undergo heterogeneous reactions at gas-solid-liquid interfaces during long-range transport [16,17]. Photochemical reductions, particularly in more acidic cloud waters

may promote dissolution of Fe [18], leading to the production of soluble Fe (II) [19–21]. Solubility of Fe could also be affected by the processes involving inorganic acidic species, such as sulfur- and nitrogen-containing compounds [22–24] and organic acidic species, such as oxalic acid [25,26]. C2–C4 dicarboxylic acids exist in the urban atmosphere [27,28], in biomass burning [29], in agricultural areas [30], over marine regions [31], and over remote regions [32]. Though they comprise a minor fraction of the total aerosol mass, these acids, in particular oxalate, play significant roles in atmospheric chemistry through complexation with metal ions (such as Fe) and in the acidity of cloud droplets and precipitation. They often exhibit different mass size distributions [33–35], and their concentrations peaked in the accumulation mode either at 0.24–0.40 or 0.40–0.80 μm aerodynamic diameters [32]. Maudlin et al. (2015) [36] conducted aerosol composition measurements at a coastal site in central California, they found that during wildfire periods, the mass size distribution of most dicarboxylic acids changed from unimodal to bimodal with peaks at 0.32 μm and 1.0–1.8 μm and Fe in sub-micrometer range was strongly enhanced. This provided evidence for the formation pathways of atmospheric particles and in Fe solubility [36–39]. Sedwick et al. (2007) [10] conducted the fractional aerosol iron solubility at the Sargasso Sea and they reported that the increased iron solubility in the aerosols was associated with North American air masses, which presented the impacts of the anthropogenic combustion products with iron that is readily soluble compared with the iron in Saharan soil dust. They implicated that atmospheric input of soluble iron to the surface ocean could be greatly affected by the anthropogenic combustion emissions.

In summary, atmospheric iron plays an important role in marine biogeochemical cycles, while iron solubility and bioavailability is highly affected by atmospheric processing. The interaction between iron speciation and other species in particles is still under investigation. Although there are many reports on atmospheric iron solubility over marine environment, few studies have been conducted in urban cities, especially in coastal areas affected by air pollution. Wang et al. (2014) [40] reported on cloud water chemical and pH measurements off the California coast during the July–August 2011 Eastern Pacific Emitted Aerosol Cloud Experiment (E-PEACE). E-PEACE results showed the evidence of micronutrients–acids interactions in the California coastal zone region, which promoted the conversion of Fe to more soluble forms during cloud processing. In brief, information is limited on how air pollution complex interacts with iron dissolution, and it is not well understood how the mass size distributions of soluble iron over coastal city regions. Newark in New Jersey on the US east coast is a metropolitan city highly impacted by air pollution and marine air. In this paper, we report and discuss the results of atmospheric iron speciation observed over the downtown Newark. Our goal is to investigate the mass size distribution of soluble iron, and to explore the interactions between soluble iron and water-soluble ionic species. Results from this work will fill the data gap in urban atmospheric iron observations and provide a wide picture of iron speciation distribution.

2. Methodology

2.1. Sampling

The sampling site was located in Newark, New Jersey on the US east coast ($40^{\circ}74' \text{ N}$, $74^{\circ}18' \text{ W}$) (Figure 1). Sampling was carried out from August to October 2012 on a platform on the roof of Bradley Hall (~20 m height above the ground) on the Newark campus of Rutgers University in downtown Newark. A 10-stage Micro-Orifice Uniform Deposit Impactor (MOUDI, MSP) with a flow rate of 30 L min^{-1} was used for sample collection, which has 50% cutoff diameters of 0.056, 0.10, 0.18, 0.32, 0.56, 1.0, 1.8, 3.2, 5.6, 10.0 and 18.0 μm . Filter changes prior to sampling and post-sampling were conducted in a 100-class laminar clean-room hood. A total of 8 sets samples (80 filters) were collected during the study period (See Table 1 for sampling information).



Figure 1. Map of the sampling site.

Table 1. Sampling information.

Set	Sampling Date	Sampling Volume (m ³)	Wind Speed (m/s)	Air Temperature (°C)	Relative Humidity (%)	Air Pressure (hPa)
No.1	08/21/2012–08/26/2012	214.2	2.5	25	63	1021
No.2	08/26/2012–08/31/2012	217.8	3.9	25	61	1017
No.3	08/31/2012–09/06/2012	236.7	3.3	25	71	1015
No.4	09/06/2012–09/11/2012	216	3.3	23	66	1013
No.5	09/21/2012–09/26/2012	215.1	3.6	19	65	1018
No.6	09/26/2012–10/01/2012	214.7	3.3	19	73	1015
No.7	10/01/2012–10/06/2012	215.1	2.8	20	78	1015
No.8	10/16/2012–10/22/2012	190.3	3.6	15	65	1012

2.2. Lab Analysis

2.2.1. Iron Speciation Analysis

Aerosol samples were analyzed for the concentrations of Fe(II) using UV/VIS spectroscopy [20,41]. The instrument used was TIDAS-1 spectrophotometer (WPI, Inc., Sarasota, FL, USA) with high sensitivity detection systems assembled by a WPI's Liquid Waveguide Capillary Cells (LWCC) with effective path lengths ranging 200 cm. The leaching method we used is the 0.5 nM ammonium acetate solution as filtered by nuclepore track-etch membrane (47 mm, 0.4 μ m, Whatman, Maidstone, UK) in the 100-class cleaning hood as the leaching solution, similar to the molar strength of the formate-acetate buffer solution utilized by Chen and Siefert (2004) [42], and the pH has been adjusted to around 5. The leaching process is ~30 min for each sample. The volume of ammonia acetate we utilized for leaching is 20 mL. To measure the iron speciation (Fe(II) and Fe(III)), the leaching solutions were split into two parts, one part was utilized for the Fe(II) measurement and the another part was utilized for the measurement of the total reduction Fe(II) (equal to Fe(TD) = Fe(II) + Fe(III)) by adding in hydroxylamine hydrochloride ($\geq 99\%$, Fisher Scientific), and the Fe(III) concentration can be calculated by subtraction the first part of Fe(II) concentration from the total Fe(II). The experiment procedures were as follows:

Each sample filter was first leached in the buffer solution of ammonia acetate for 1 h and the leaching solution was split into two parts. The first part (9.5 mL) was added in the 0.5 mL 0.01 M of the color complex ferrozine solution and the final volume was 10 mL. At the same time, the second part (7.5 mL) was added in 2 mL of the 0.01 M hydroxylamine solution to reduce Fe(III) to Fe(II), staying for 30 min and then the 0.5 mL 0.01 M of the ferrozine solution was added and the final

volume was also 10 mL. All the solutions have been filtered with 13 mm PTFE syringe filter with pore size of 0.2 μm . Then the concentrations of Fe(II) were determined at 562 nm by a modified ferrozine procedure [20,42–44]. The limits of detection (LODs), estimated as three times the standard deviation of the measurement blanks ($n = 5$ for Fe(II)), were 0.26 nM. The blank was 2.6 nM ($n = 5$).

2.2.2. IC Analysis

The analysis of selected water soluble ion species in samples was completed by a Dionex ICS-2000 IC in the Atmosphere Chemistry Lab of Rutgers University at Newark. The major inorganic ions include Na^+ , NH_4^+ , K^+ , Mg^{2+} , Ca^{2+} , Cl^- , NO_3^- , SO_4^{2-} , and Oxalate ($\text{C}_2\text{O}_4^{2-}$). All anion species were analyzed with an AS11 analytical column, KOH eluent generator cartridge and 25 μL sample loop, while all cations were analyzed with a CS12A analytical column, MSA generator cartridge and 25 μL sample loop. Operation procedures were as following: A 1/4 portion of each filter was placed in 15 mL of deionized water, with ultra-sonication for one hour and four hours' leaching. Then the sample solutions were injected into the IC system through filters with 0.22 μm pore diameter. The detection limit for major anions, including sulfate, nitrate, chloride, oxalate is $<9 \mu\text{g L}^{-1}$. The recovery falls in the range of 78%–101%. Based on seven duplicate spike samples, the precision of the analytical procedures is $\sim 1\%$. Detailed information of the method is given in Zhao and Gao (2008) [28]. Final concentrations of these species were obtained after correction with field blanks, and their standard deviations were below 0.01.

3. Meteorological Data

During sampling periods, the meteorological data including air temperature, air pressure, relative humidity, and wind speed were obtained from a nearby weather station at Newark Museum and can be received online [45] (see Table 1). To explore the potential sources of air masses, the air mass back-trajectories (AMBTs) were calculated from the National Oceanic and Atmospheric Administration (NOAA) GDAS meteorology database using the Hybrid Single-Particle Lagrangian Integrated Trajectories (HY-SPLIT) program. AMBTs were performed at 20, 500 and 2000 m height levels over the sampling locations every six hours with backward ~ 5 days by considering the sampling duration and the aerosol residence time in the atmosphere during its transportation to figure out where air mass came from (Figure 2).

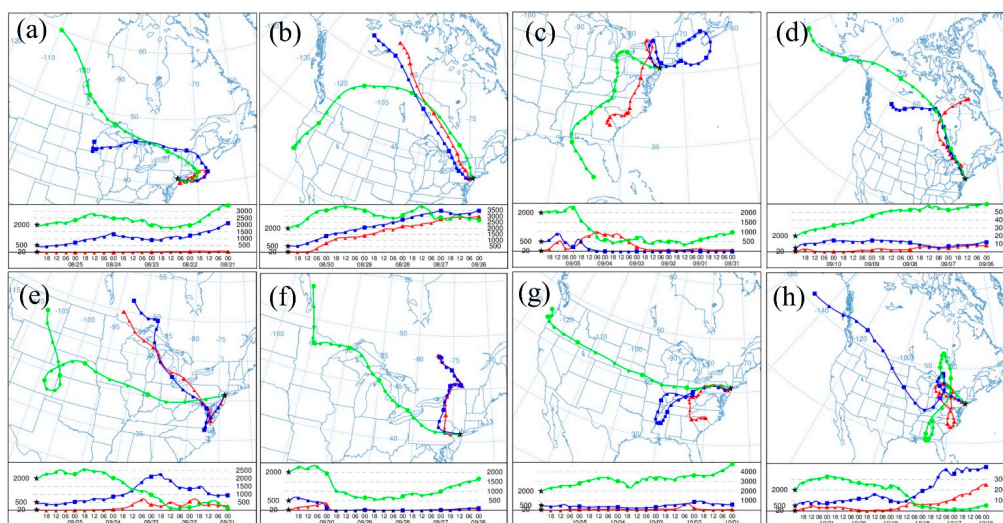


Figure 2. Air mass back-trajectories for each sample at the ending date of sampling at heights of 20 m, 500 m and 2000 m: (a) Sample No.1; (b) Sample No.2; (c) Sample No.3; (d) Sample No.4; (e) Sample No.5; (f) Sample No.6; (g) Sample No.7; and (h) Sample No.8. The back-trajectories were calculated using NOAA HYSPLIT Model [46].

4. Results and Discussion

4.1. Iron Speciation

The concentrations of Fe(II) ranged from 1.2 to 4.2 ng m⁻³ (average: 2.1 ng m⁻³) and Fe(TD) ranged from 1.3 ng m⁻³ to 4.9 ng m⁻³ (average: 2.4 ng m⁻³) over US east coast Newark site. Sample No.7 with the highest Fe(II) and Fe(TD) concentration was associated with high sulfate, oxalate and nitrate concentrations. The air mass back trajectories of Sample No.7 showed that high dissolved iron was associated with air masses passing over US southwest; especially at 2000 m height, the air mass came from American west, where the weather was dry and much dust suspended in the air (Figure 2).

Atmospheric dissolved Fe has been measured over the oceans, including the Indian Ocean [47,48], the Atlantic Ocean [10,43,49–51], the Pacific Ocean [43,52] and the Southern Ocean [41] (Table 2). Results from this study over the US east coast were generally comparable to those over marine environments, especially the investigation conducted over the North Atlantic. However, the highest total dissolved iron from this study was lower than that over the Northwest Pacific and East China Sea [43,53], where there were large amounts of dust, internally mixing with anthropogenic air pollutants [18], while it was higher than the observation results over the pristine environment, such as the coastal East Antarctica [41].

Table 2. Comparison of Fe(II) and Fe(TD) concentrations at different locations.

Locations	Latitude/Longitude	Fe(II) (ng m ⁻³)	Fe(TD) (ng m ⁻³)	Citations
Northwest Pacific	50° N–24° N, 170° E	0.05–5.3	0.28–86	Buck et al. (2006) [43]
East China Sea	25° N–30° N, 120° E–127° E		1.7–120	Hsu et al. (2009) [53]
North Atlantic	13.17° N, 59.43° W	2.5 ± 1.8 (0.63–8.2)	12 ± 8.4 (2.8–33)	Zhu et al. (1997) [20]
North Atlantic	10° N–30° N, 30° W–60° W	0.19–1.2	0.35–20	Chen and Siefert (2004) [42]
North Atlantic	~30° N–31.5° N, ~63.5° W–65.5° W		4.5–12	Sedwick et al. (2007) [10]
Coastal East Antarctic	64° S–69° S 75° E–110° E	0.53 ± 0.38 (0.18–1.3)	1.2 ± 1.1 (0.23–3.3)	Gao et al. (2013) [41]
US Northeast Coast Newark	40°74' N 74°18' W	2.1 (1.2–4.2)	2.4 (1.3–4.9)	This study

4.2. Particle Size Distribution

4.2.1. Fe(II) and Fe(TD)

Figure 3a showed the particle size distribution of Fe(II). A bi-modal size distribution of Fe(II) was observed with seven sets of size-segregated aerosol samples (No.1–No.6, and No.8), while Sample No.7 has a single fine mode distribution (defined as particles with cutoff diameter ≤ 2.5 μm). The highest Fe(II) concentration was associated with the fine-mode particles, with particles size range 1.0–1.4 μm. A similar size distribution pattern was shown in Fe(TD) (Figure 3b). Siefert et al. (1999) [47] conducted the observation over the Arabian Sea during the southwest monsoon and inter-monsoon seasons. They found that the iron portion in particles with diameter smaller than 3 μm is larger than that of diameter larger than 3 μm, which may be explained by the anthropogenic sources accumulated in the small particle size range and produce more soluble iron. Gao et al. (2013) [41] collected size-segregated aerosol samples over the Southern Ocean and coastal East Antarctica, and found that Fe(II) dominantly appeared in particle size ≤ 1 μm, even though bi-modal size distribution of Fe(II) was shown in coastal East Antarctica due to potential dust sources in Antarctica. Compared to the pristine environment,

our results on the US east coast suggested that atmospheric dissolved iron in urban city may not only be influenced by urban traffic activities, but also affected by suspended road dust.

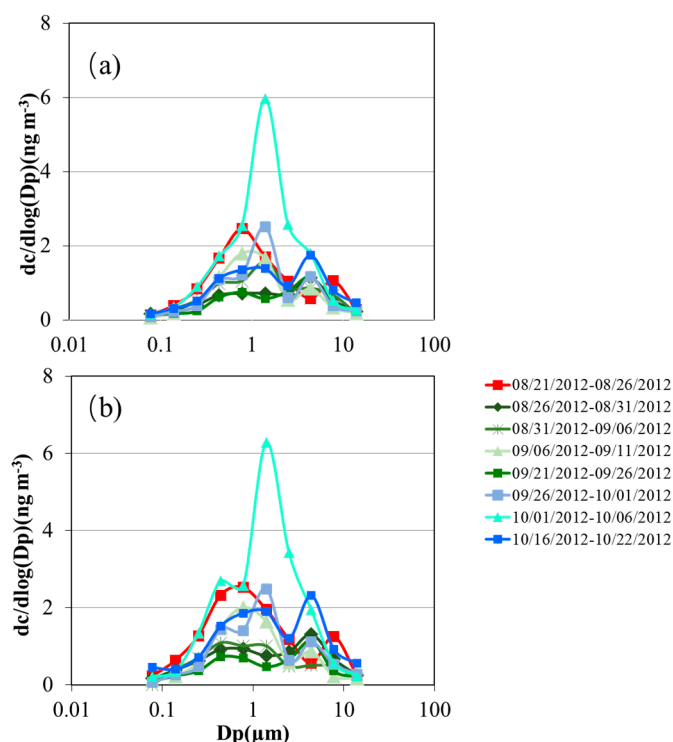


Figure 3. Particle size distribution of: (a) Fe(II); and (b) Fe(TD).

4.2.2. NH_4^+ , NO_3^- , SO_4^{2-} , Oxalate

The size distribution of NH_4^+ (Figure 4a) mainly peaked at 0.32–0.56 μm , except Sample No.7, which was accumulated in size range 1.0–1.8 μm . The enrichment of NH_4^+ in the fine mode can be explained by chemical reactions between gaseous precursor NH_3 and acidic species through gas phase and aqueous reactions [54]. Figure 4b displays coarse mode (defined as particles with cutoff diameter $\geq 2.5 \mu\text{m}$) distribution of NO_3^- , except Sample No.7 appears in bi-modal size distribution. Coarse-mode nitrate is mainly formed through nitric acid related chemical reactions on particle surface [55]. Figure 4c shows that SO_4^{2-} was mainly accumulated in 0.32–0.56 μm , which was consistent with the size distribution of NH_4^+ , suggesting that the potential formation of NH_4HSO_4 and $(\text{NH}_4)_2\text{SO}_4$ in aerosols. Fan et al. (2006) [23] found that the coating of dust particles by sulfate from ambient trace gas deposition was likely the main factor for the enhanced fertilization of the modern northern hemisphere ocean. Organic acids such as low molecular weight dicarboxylic acids with low vapor pressure are soluble in aqueous solution, are consequently strongly hygroscopic [56], thus, when accumulated in sufficient quantity, have a much greater ability than the inorganic species SO_4^{2-} and NO_3^- to lower the surface tension of cloud condensation nuclei (CCN). Through this action, they have a significant potential on acid processing [57]. In this study, oxalate displayed a bi-modal size distribution, mainly in particle size range 0.32–0.56 μm . Hence, the existence of a large amount of oxalate in the accumulation mode could interact with dissolved iron through chemical reactions during transport. This will be discussed in Section 4.3.

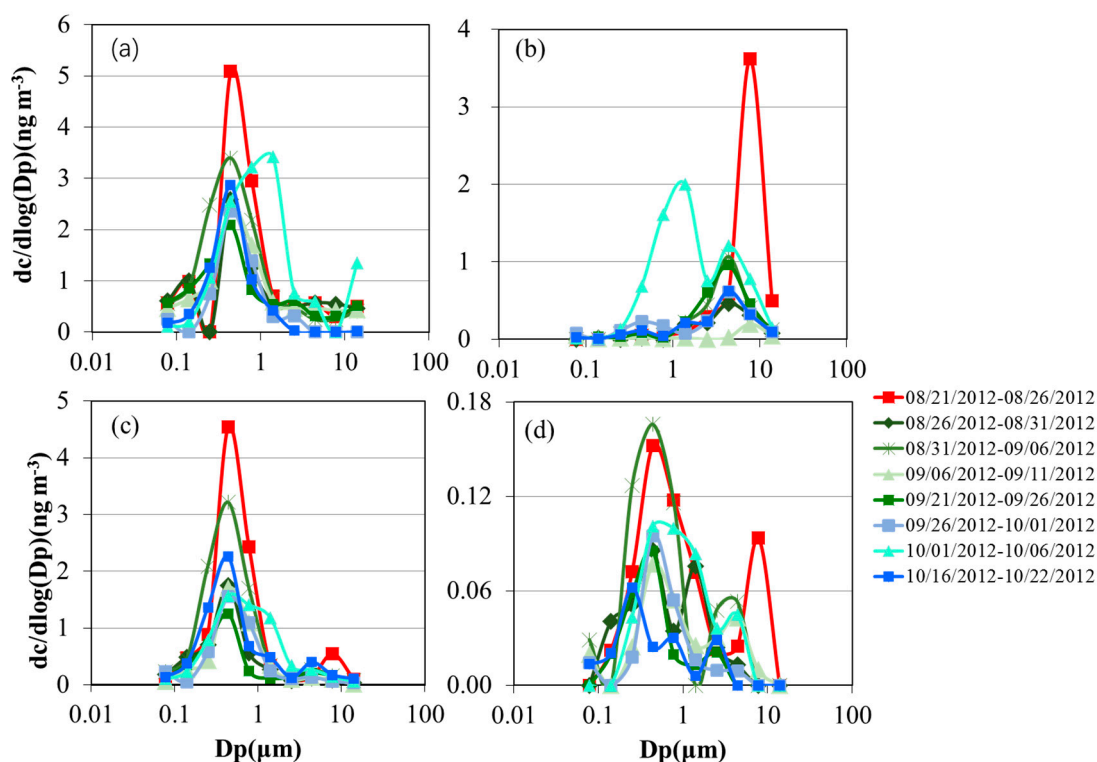


Figure 4. Particle size distribution of: (a) NH_4^+ ; (b) NO_3^- ; (c) SO_4^{2-} ; and (d) Oxalate.

4.3. Acid Processing

There were various controlling factors of the Fe solubility, and, among them, acid processing was possibly the dominant factor. Solmon et al. (2009) [58] conducted the mineral dust iron research over the North Pacific Ocean and found that insoluble iron in mineral dust could become soluble, as anthropogenic pollutants play an important role, such as the acid processing involved. They found that there was a good correlation between the dust-soluble iron and pollutants, and chemical processing mechanism could produce significant amounts of dissolved iron that could be transported and deposited in remote regions of the Pacific basin.

To explore how acid processing affect iron solubility, correlations between dissolved iron (Fe(II) and Fe(TD)) and inorganic and organic acids were calculated (Figure 5). Results showed that there was a significant good correlation ($p < 0.05$, $R > 0.5$, $n = 8$) between dissolved iron (Fe(II) and Fe(TD)) and sulfate in the coarse mode, but there was no good correlation between dissolved iron and oxalate in both mode, which may result from the low concentration of oxalate in the ambient environment. Sorooshian et al. (2013) [59] conducted field work in northeastern Pacific Ocean by collecting stratocumulus cloud water and examining the organic acid and metal concentrations; they found an inverse relationship between oxalate and Fe. Thus, the oxalate sink in this study could be explained to some extent by the photolysis of iron oxalato complexes. A significant good correlation ($p < 0.05$, $R > 0.5$, $n = 8$) between dissolved iron and nitrate in the coarse mode was found, indicating that if nitrate concentration increased, dissolved iron concentration also increased. Hsu et al. (2010) [60] collected aerosols over the East China Sea and the water-soluble iron, total iron and other water soluble species have been analyzed, and they found that soluble Fe correlated well with non-sea-salt sulfate, water-soluble organic carbon, and nitrate, which indicated that anthropogenic sources of soluble iron or pollutant acids may be involved in the iron dissolution enhancement reactions. In this study, good correlation between coarse mode sulfate, fine mode nitrate and dissolved iron in the atmosphere revealed the acid processing involved in the iron dissolution enhancement reactions. Dall'Osto et al. (2016) [61] collected Fe-containing particles at two European urban sites and found that Fe aerosols

were internally mixed with nitrate but not with sulfate, which highlighted the contribution from urban traffic activities in European, not like coal combustion origin in Asia. In addition, our study could not support the theory of complexation of Fe(III) by organic ligands such as formate, acetate and oxalate, during which the photo-production of more soluble Fe(II) was promoted, with the organic ligand acting as the electron donor [62,63]. One possible reason is that the low concentration of organic acids may not be enough to react with Fe(III) to form Fe(II).

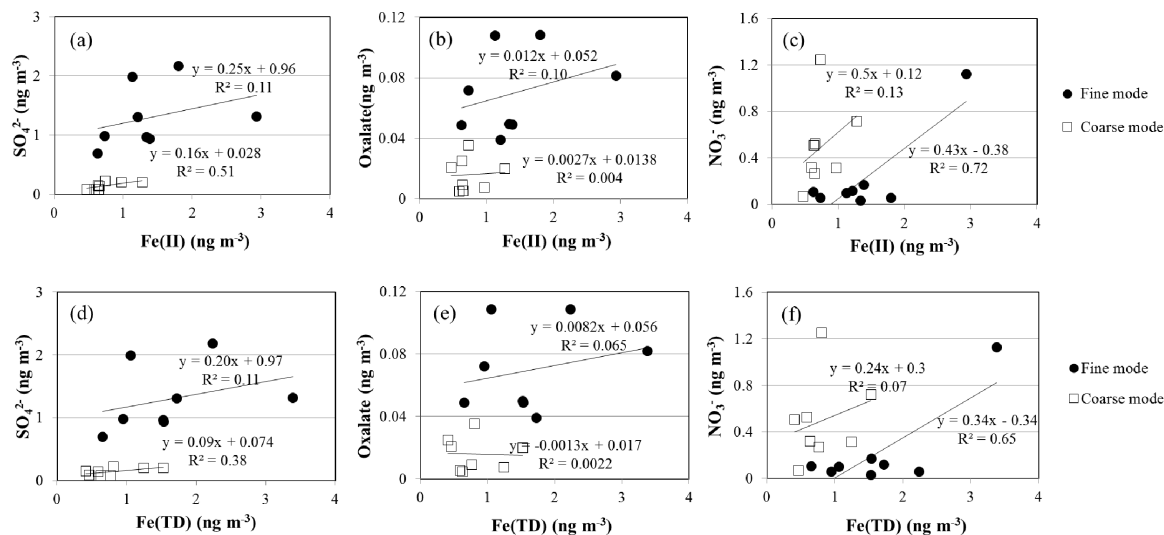


Figure 5. Correlation between dissolved iron (Fe(II), Fe(TD)), Sulfate, Oxalate and Nitrate: (a) Fe(II) and SO₄²⁻; (b) Fe(II) and Oxalate; (c) Fe(II) and NO₃⁻; (d) Fe(TD) and SO₄²⁻; (e) Fe(TD) and Oxalate; and (f) Fe(TD) and NO₃⁻.

On the other side, it was impossible to isolate the fraction of dissolved iron directly emitted with anthropogenic sources from the fraction of dust dissolved iron formed in acidic air masses rich in anthropogenic pollutants, so the correlation between iron solubility and other acid species was complicated, which may not be simply presented as a linear correlation [64]. Other factors may also affect the iron dissolution reactions: Luo et al. (2005) [65] concluded that in-cloud processing was a dominant factor for iron dissolution. In-cloud photochemical processes reducing iron to a more soluble state (Fe(II)) have been the focus of several experiments. These studies have shown that aqueous complexes between Fe(III) and specific organic and inorganic ligands can play an important role in the photo-reduction of Fe(III) to Fe(II) in cloud water or deliquesced aerosols. The steady state concentrations of Fe(II) are strongly dependent on the pH of solution and the available solar radiation.

5. Conclusions

Results from this study on particle size distributions of dissolved iron and water-soluble aerosol species in metropolitan Newark on the US east coast leads to the following conclusions.

Ambient dissolved iron (Fe(II) and Fe(TD)) concentrations were comparable to the observation results conducted over marine environments, especially the results over the North Atlantic.

Particle size distribution of dissolved iron in general appeared as bi-modal size distribution, but was mainly accumulated in the fine mode. The highest concentration of dissolved iron displayed in the fine mode may suggest the potential for Fe-acids interactions in the fine mode particles. NH₄⁺ and SO₄²⁻ displayed a similar size distribution pattern in the fine mode, while NO₃⁻ was mainly accumulated in the coarse mode. The oxalate concentration was low and appeared as a bi-modal size distribution pattern.

Good correlation was found between dissolved iron and sulfate in the coarse mode, and between dissolved iron and nitrate in the fine mode. It suggested the importance of acid processing in changing

the iron solubility. However, a good correlation between dissolved iron and oxalate was not found in both fine and coarse mode particles collected on US east coast. A possible reason was that organic acids concentration was too low to interact with iron.

Acknowledgments: This work was funded by the Startup Foundation for Introducing Talent of NUIST, and the Double Innovation Talent Program. The authors thank Rafael Jusino-Atresino for assistance in maintaining the sampling platform at the Newark site and for valuable discussions, and Jianqiong Zhan for assistant with IC lab analysis.

Author Contributions: Yuan Gao designed and supervised the research. Guojie Xu collected samples, analyzed the samples and processed the data. Guojie Xu and Yuan Gao wrote the manuscript.

Conflicts of Interest: The authors declare no conflict of interest.

References

1. Sunda, W. Bioavailability and bioaccumulation of iron in the sea. In *the Biogeochemistry of Iron in Seawater*; Turner, D.R., Hunter, K., Eds.; John Wiley: New York, NY, USA, 2001; pp. 41–84.
2. Duce, R.A.; Liss, P.S.; Merrill, J.T.; Atlas, E.L.; Buat-Menard, P.; Hicks, B.B.; Miller, J.M.; Prospero, J.M.; Arimoto, R.; Church, T.M. The atmospheric input of trace species to the world ocean. *Global Biogeochem. Cycles* **1991**, *5*, 193–259. [[CrossRef](#)]
3. Gao, Y.; Kaufman, Y.J.; Tanré, D.; Kolber, D.; Falkowski, P.G. Seasonal distributions of aeolian iron fluxes to the global ocean. *Geophys. Res. Lett.* **2001**, *28*, 29–32. [[CrossRef](#)]
4. Prospero, J.M.; Ginoux, P.; Torres, O.; Nicholson, S.E.; Gill, T.E. Environmental characterization of global sources of atmospheric soil dust identified with the Nimbus 7 Total Ozone Mapping Spectrometer (TOMS) absorbing aerosol product. *Rev. Geophys.* **2002**, *40*. [[CrossRef](#)]
5. Li, F.; Ginoux, P.; Ramaswamy, V. Distribution, transport, and deposition of mineral dust in the Southern Ocean and Antarctica: Contribution of major sources. *J. Geophys. Res. Atmos.* **2008**, *113*. [[CrossRef](#)]
6. Guieu, C.; Bonnet, S.; Wagener, T.; Loÿe-Pilot, M.D. Biomass burning as a source of dissolved iron to the open ocean? *Geophys. Res. Lett.* **2005**, *32*, 205–213. [[CrossRef](#)]
7. Fu, H.B.; Shang, G.F.; Lin, J.; Hu, Y.J.; Hu, Q.Q.; Guo, L.; Zhang, Y.C.; Chen, J.M. Fractional iron solubility of aerosol particles enhanced by biomass burning and ship emission in Shanghai, East China. *Sci. Total Environ.* **2014**, *481*, 377–391. [[CrossRef](#)] [[PubMed](#)]
8. Fu, H.; Lin, J.; Shang, G.; Dong, W.; Grassian, V.H.; Carmichael, G.R.; Li, Y.; Chen, J. Solubility of iron from combustion source particles in acidic media linked to iron speciation. *Environ. Sci. Technol. Lett.* **2012**, *46*, 11119–11127. [[CrossRef](#)] [[PubMed](#)]
9. Chuang, P.; Duvall, R.; Shafer, M.; Schauer, J. The origin of water soluble particulate iron in the Asian atmospheric outflow. *Geophys. Res. Lett.* **2005**, *32*. [[CrossRef](#)]
10. Sedwick, P.N.; Sholkovitz, E.R.; Church, T.M. Impact of anthropogenic combustion emissions on the fractional solubility of aerosol iron: Evidence from the Sargasso Sea. *Geochem. Geophys. Geosyst.* **2007**, *8*. [[CrossRef](#)]
11. Luo, C.; Mahowald, N.; Bond, T.; Chuang, P.; Artaxo, P.; Siefert, R.; Chen, Y.; Schauer, J. Combustion iron distribution and deposition. *Global Biogeochem. Cycles* **2008**, *22*. [[CrossRef](#)]
12. Jickells, T.D.; Spokes, L.J. Atmospheric iron inputs to the oceans. In *The Biogeochemistry of Iron in Seawater*; Turner, D.R., Hunter, K., Eds.; John Wiley & Sons, Inc.: New York, NY, USA, 2001; pp. 85–121.
13. Johansen, A.M.; Siefert, R.L.; Hoffmann, M.R. Chemical composition of aerosols collected over the tropical North Atlantic Ocean. *J. Geophys. Res. Atmos.* **2000**, *105*, 15277–15312. [[CrossRef](#)]
14. Baker, A.; Jickells, T. Mineral particle size as a control on aerosol iron solubility. *Geophys. Res. Lett.* **2006**, *33*. [[CrossRef](#)]
15. Schroth, A.W.; Crusius, J.; Sholkovitz, E.R.; Bostick, B.C. Iron solubility driven by speciation in dust sources to the ocean. *Nat. Geosci.* **2009**, *2*, 337–340. [[CrossRef](#)]
16. Dentener, F.J.; Carmichael, G.R.; Zhang, Y.; Lelieveld, J.; Crutzen, P.J. Role of mineral aerosol as a reactive surface in the global troposphere. *J. Geophys. Res. Atmos.* **1996**, *101*, 22869–22889. [[CrossRef](#)]
17. Underwood, G.; Song, C.; Phadnis, M.; Carmichael, G.; Grassian, V. Heterogeneous reactions of NO₂ and HNO₃ on oxides and mineral dust: A combined laboratory and modeling study. *J. Geophys. Res. Atmos.* **2001**, *106*, 18055–18066. [[CrossRef](#)]

18. Li, W.; Xu, L.; Liu, X.; Zhang, J.; Lin, Y.; Yao, X.; Gao, H.; Zhang, D.; Chen, J.; Wang, W.; et al. Air pollution-aerosol interactions produce more bioavailable iron for ocean ecosystems. *Sci. Adv.* **2017**, *3*. [[CrossRef](#)] [[PubMed](#)]
19. Faust, B.C.; Zepp, R.G. *Photochemistry of Aqueous Iron (III)-Polycarboxylate Complexes: Roles in the Chemistry of Atmospheric And Surface Waters*; Environmental Protection Agency: Athens, GA, USA, January 1993.
20. Zhu, X.; Prospero, J.; Millero, F. Diel variability of soluble Fe (II) and soluble total Fe in North African dust in the trade winds at Barbados. *J. Geophys. Res. Biogeosci.* **1997**, *102*, 21297–221305. [[CrossRef](#)]
21. Kieber, R.J.; Hardison, D.; Whitehead, R.F.; Willey, J.D. Photochemical production of Fe (II) in rainwater. *Environ. Sci. Technol. Lett.* **2003**, *37*, 4610–4616. [[CrossRef](#)]
22. Meskhidze, N.; Chameides, W.; Nenes, A.; Chen, G. Iron mobilization in mineral dust: Can anthropogenic SO₂ emissions affect ocean productivity? *Geophys. Res. Lett.* **2003**, *30*. [[CrossRef](#)]
23. Fan, S.M.; Moxim, W.J.; Levy, H. Aeolian input of bioavailable iron to the ocean. *Geophys. Res. Lett.* **2006**, *33*. [[CrossRef](#)]
24. Yang, H.; Gao, Y. Air-to-sea flux of soluble iron: Is it driven more by HNO₃ or SO₂?—An examination in the light of dust aging. *Atmos. Chem. Phys. Discuss.* **2007**, *7*, 10043–10063. [[CrossRef](#)]
25. Xu, N.; Gao, Y. Characterization of hematite dissolution affected by oxalate coating, kinetics and pH. *Appl. Geochem.* **2008**, *23*, 783–793. [[CrossRef](#)]
26. Luo, C.; Gao, Y. Aeolian iron mobilisation by dust-acid interactions and their implications for soluble iron deposition to the ocean: A test involving potential anthropogenic organic acidic species. *Environ. Chem.* **2010**, *7*, 153–161. [[CrossRef](#)]
27. Kawamura, K.; Ikushima, K. Seasonal changes in the distribution of dicarboxylic acids in the urban atmosphere. *Environ. Sci. Technol.* **1993**, *27*, 2227–2235. [[CrossRef](#)]
28. Zhao, Y.; Gao, Y. Mass size distributions of water-soluble inorganic and organic ions in size-segregated aerosols over metropolitan Newark in the US east coast. *Atmos. Environ.* **2008**, *42*, 4063–4078. [[CrossRef](#)]
29. Prabhakar, G.; Ervens, B.; Wang, Z.; Maudlin, L.C.; Coggon, M.M.; Jonsson, H.H.; Seinfeld, J.H.; Sorooshian, A. Sources of nitrate in stratocumulus cloud water: Airborne measurements during the 2011 E-PEACE and 2013 NICE studies. *Atmos. Environ.* **2014**, *97*, 166–173. [[CrossRef](#)]
30. Sorooshian, A.; Murphy, S.M.; Hersey, S.; Gates, H. Comprehensive airborne characterization of aerosol from a major bovine source. *Atmos. Chem. Phys.* **2008**, *8*, 5489–5520. [[CrossRef](#)]
31. Sorooshian, A.; Murphy, S.M.; Hersey, S.; Bahreini, R.; Jonsson, H.; Flagan, R.C.; Seinfeld, J.H. Constraining the contribution of organic acids and AMS m/z 44 to the organic aerosol budget: On the importance of meteorology, aerosol hygroscopicity, and region. *Geophys. Res. Lett.* **2010**, *37*. [[CrossRef](#)]
32. Kawamura, K.; Narukawa, M.; Li, S.M.; Barrie, L.A. Size distributions of dicarboxylic acids and inorganic ions in atmospheric aerosols collected during polar sunrise in the Canadian high arctic. *J. Geophys. Res. Atmos.* **2007**, *112*. [[CrossRef](#)]
33. Whitby, K.T. The physical characteristics of sulfur aerosols. *Atmos. Environ.* **1978**, *12*, 135–159. [[CrossRef](#)]
34. Mochida, M.; Kawabata, A.; Kawamura, K.; Hatsushika, H.; Yamazaki, K. Seasonal variation and origins of dicarboxylic acids in the marine atmosphere over the western North Pacific. *J. Geophys. Res. Atmos.* **2003**, *108*. [[CrossRef](#)]
35. Cabada, J.C.; Pandis, S.N.; Subramanian, R.; Robinson, A.L.; Polidori, A.; Turpin, B. Estimating the secondary organic aerosol contribution to PM_{2.5} using the EC tracer method special issue of aerosol science and technology on findings from the fine particulate matter supersites program. *Aerosol Sci. Technol.* **2004**, *38*, 140–155. [[CrossRef](#)]
36. Maudlin, L.C.; Wang, Z.; Jonsson, H.H.; Sorooshian, A. Impact of wildfires on size-resolved aerosol composition at a coastal California site. *Atmos. Environ.* **2015**, *119*, 59–68. [[CrossRef](#)]
37. Meng, Z.; Seinfeld, J.H. On the source of the submicrometer droplet mode of urban and regional aerosols. *Aerosol Sci. Technol.* **1994**, *20*, 253–265. [[CrossRef](#)]
38. Kerminen, V.M.; Wexler, A.S. Growth laws for atmospheric aerosol particles: An examination of the bimodality of the accumulation mode. *Atmos. Environ.* **1995**, *29*, 3263–3275. [[CrossRef](#)]
39. Kerminen, V.-M.; Ojanen, C.; Pakkanen, T.; Hillamo, R.; Aurela, M.; Meriläinen, J. Low-molecular-weight dicarboxylic acids in an urban and rural atmosphere. *J. Aerosol Sci.* **2000**, *31*, 349–362. [[CrossRef](#)]

40. Wang, Z.; Sorooshian, A.; Prabhakar, G.; Coggon, M.M.; Jonsson, H.H. Impact of emissions from shipping, land, and the ocean on stratocumulus cloud water elemental composition during the 2011 E-PEACE field campaign. *Atmos. Environ.* **2014**, *89*, 570–580. [[CrossRef](#)]
41. Gao, Y.; Xu, G.; Zhan, J.; Zhang, J.; Li, W.; Lin, Q.; Chen, L.; Lin, H. Spatial and particle size distributions of atmospheric dissolvable iron in aerosols and its input to the Southern Ocean and coastal East Antarctica. *J. Geophys. Res. Atmos.* **2013**, *118*. [[CrossRef](#)]
42. Chen, Y.; Siefert, R.L. Seasonal and spatial distributions and dry deposition fluxes of atmospheric total and labile iron over the tropical and subtropical North Atlantic Ocean. *J. Geophys. Res. Atmos.* **2004**, *109*. [[CrossRef](#)]
43. Buck, C.S.; Landing, W.M.; Resing, J.A.; Lebon, G.T. Aerosol iron and aluminum solubility in the northwest Pacific Ocean: Results from the 2002 IOC cruise. *Geochem. Geophys. Geosyst.* **2006**, *7*. [[CrossRef](#)]
44. Xia, L.; Gao, Y. Chemical composition and size distributions of coastal aerosols observed on the us east coast. *Mar. Chem.* **2010**, *119*, 77–90. [[CrossRef](#)]
45. The Weather Company. Available online: <https://www.wunderground.com/> (accessed on 7 March 2017).
46. Air Resources Laboratory. Available online: http://www.arl.noaa.gov/HYSPLIT_info.php (accessed on 7 March 2017).
47. Siefert, R.L.; Johansen, A.M.; Hoffmann, M.R. Chemical characterization of ambient aerosol collected during the southwest monsoon and intermonsoon seasons over the Arabian Sea: Labile-Fe (II) and other trace metals. *J. Geophys. Res. Atmos.* **1999**, *104*, 3511–3526. [[CrossRef](#)]
48. Johansen, A.M.; Hoffmann, M.R. Chemical characterization of ambient aerosol collected during the northeast monsoon season over the Arabian Sea: Labile-Fe (II) and other trace metals. *J. Geophys. Res. Atmos.* **2003**, *108*. [[CrossRef](#)]
49. Baker, A.; Kelly, S.; Biswas, K.; Witt, M.; Jickells, T. Atmospheric deposition of nutrients to the Atlantic Ocean. *Geophys. Res. Lett.* **2003**, *30*. [[CrossRef](#)]
50. Kramer, J.; Laan, P.; Sarthou, G.; Timmermans, K.; De Baar, H. Distribution of dissolved aluminium in the high atmospheric input region of the subtropical waters of the North Atlantic Ocean. *Mar. Chem.* **2004**, *88*, 85–101. [[CrossRef](#)]
51. Sedwick, P.N.; Church, T.M.; Bowie, A.R.; Marsay, C.M.; Ussher, S.J.; Achilles, K.; Lethaby, P.; Johnson, R.J.; Sarin, M.; McGillicuddy, D.J. Iron in the Sargasso Sea (Bermuda Atlantic Time-series Study region) during summer: Eolian imprint, spatiotemporal variability, and ecological implications. *Global Biogeochem. Cycles* **2005**, *19*. [[CrossRef](#)]
52. Measures, C.; Cutter, G.; Landing, W.; Powell, R. Hydrographic observations during the 2002 IOC contaminant baseline survey in the western Pacific Ocean. *Geochem. Geophys. Geosystems.* **2006**, *7*. [[CrossRef](#)]
53. Hsu, S.C.; Liu, S.C.; Arimoto, R.; Liu, T.H.; Huang, Y.T.; Tsai, F.; Lin, F.J.; Kao, S.J. Dust deposition to the East China Sea and its biogeochemical implications. *J. Geophys. Res. Atmos.* **2009**, *114*. [[CrossRef](#)]
54. Zhang, L.; Vet, R.; Wiebe, A.; Mihele, C.; Sukloff, B.; Chan, E.; Moran, M.; Iqbal, S. Characterization of the size-segregated water-soluble inorganic ions at eight Canadian rural sites. *Atmos. Chem. Phys.* **2008**, *8*, 7133–7151. [[CrossRef](#)]
55. Anlauf, K.; Li, S.-M.; Leaitch, R.; Brook, J.; Hayden, K.; Toom-Sauntry, D.; Wiebe, A. Ionic composition and size characteristics of particles in the lower fraser valley: Pacific 2001 field study. *Atmos. Environ.* **2006**, *40*, 2662–2675. [[CrossRef](#)]
56. Yu, J.; Flagan, R.C.; Seinfeld, J.H. Identification of products containing –COOH, –OH, and –CO in atmospheric oxidation of hydrocarbons. *Environ. Sci. Technol.* **1998**, *32*, 2357–2370. [[CrossRef](#)]
57. Kasper-Giebl, A.; Bauer, H.; Giebl, H.; Hitzenberger, R.; Löflund, M.; Puxbaum, H. *Transport and Chemical Transformation in the Troposphere*; Springer: Berlin, Germany, 2002.
58. Solmon, F.; Chuang, P.; Meskhidze, N.; Chen, Y. Acidic processing of mineral dust iron by anthropogenic compounds over the north Pacific Ocean. *J. Geophys. Res. Atmos.* **2009**, *114*. [[CrossRef](#)]
59. Sorooshian, A.; Wang, Z.; Coggon, M.M.; Jonsson, H.H.; Ervens, B. Observations of sharp oxalate reductions in stratocumulus clouds at variable altitudes: Organic acid and metal measurements during the 2011 E-PEACE campaign. *Environ. Sci. Technol.* **2013**, *47*, 7747–7756. [[CrossRef](#)] [[PubMed](#)]
60. Hsu, S.C.; Wong, G.T.; Gong, G.C.; Shiah, F.K.; Huang, Y.T.; Kao, S.J.; Tsai, F.; Lung, S.C.C.; Lin, F.J.; Lin, I. Sources, solubility, and dry deposition of aerosol trace elements over the East China Sea. *Mar. Chem.* **2010**, *120*, 116–127. [[CrossRef](#)]

61. Dall'Osto, M.; Beddows, D.C.; Harrison, R.M.; Onat, B. Fine iron aerosols are internally mixed with nitrate in the urban European atmosphere. *Environ. Sci. Technol.* **2016**, *50*, 4212–4220. [[CrossRef](#)] [[PubMed](#)]
62. Pehkonen, S.O.; Siefert, R.; Erel, Y.; Webb, S.; Hoffmann, M.R. Photoreduction of iron oxyhydroxides in the presence of important atmospheric organic compounds. *Environ. Sci. Technol.* **1993**, *27*, 2056–2062. [[CrossRef](#)]
63. Siefert, R.L.; Pehkonen, S.O.; Erel, Y.; Hoffmann, M.R. Iron photochemistry of aqueous suspensions of ambient aerosol with added organic acids. *Geochim. Cosmochim. Acta.* **1994**, *58*, 3271–3279. [[CrossRef](#)]
64. Moffet, R.C.; Furutani, H.; Rödel, T.C.; Henn, T.R.; Sprau, P.O.; Laskin, A.; Uematsu, M.; Gilles, M.K. Iron speciation and mixing in single aerosol particles from the Asian continental outflow. *J. Geophys. Res. Atmos.* **2012**, *117*. [[CrossRef](#)]
65. Luo, C.; Mahowald, N.; Meskhidze, N.; Chen, Y.; Siefert, R.; Baker, A.; Johansen, A. Estimation of iron solubility from observations and a global aerosol model. *J. Geophys. Res. Atmos.* **2005**, *110*. [[CrossRef](#)]



© 2017 by the authors. Licensee MDPI, Basel, Switzerland. This article is an open access article distributed under the terms and conditions of the Creative Commons Attribution (CC BY) license (<http://creativecommons.org/licenses/by/4.0/>).